Control-based Fault Current Limiter for Minimizing Impact of Distributed Generation Units on Protection Systems

Pablo E. Muñoz, Ricardo J. Mantz, and Sergio A. González

***Abstract*—Distributed generation units (DGUs) bring some problems to the existing protection system, such as those associated with protection blinding and sympathetic tripping. It is known that fault current limiters (FCLs) help minimize the negative impact of DGUs on the protection system. In this paper, a control-based FCL is proposed, i.e., the FCL is integrated into the DGU control law. To this end, a predictive control strategy with fault current limitation is suggested. In this way, a DGU is controlled, not only for power exchange with the power grid but also to limit its fault current contribution. The proposal is posed as a constrained optimization problem allowing taking into account the current limit explicitly in the design process as a closed-loop solution. A linear approximation is proposed to cope with the inherent nonlinear constraints. The proposal does not require incorporating extra equipment or mechanisms in the control loop, making the design process simple. To evaluate the proposed control-based FCL, both protection blinding and sympathetic tripping scenarios are considered. The control confines the DGU currents within the constraints quickly, avoiding large transient peaks. Therefore, the impact on the protection system is reduced without the necessity that the DGU goes out of service.**

***Index Terms*—Distributed generation, distribution network, protection, power electronic converter, fault current limiter, model-based predictive controller.**

I. Introduction

In the coming years, the penetration of renewable energies in the power system will be higher in order to achieve a sustainable power system. In this context, the distributed generation units (DGUs) connected to the power grid will increase in the near future. DGUs can be conventional generators or renewable energy sources (RESs) connected by power electronic converters (PECs) to the distribution networks or at the customer side of the network [1]. PECs are used as interfaces in DGUs because they allow adapting the power generated by the RES to the needs of the power grid and their high efficiency [2].

Distributed generation (DG) introduces several improvements to the distribution network such as the reduction of transmission losses, power quality improvement, and increase in system reliability. However, high penetration of DG brings new protection problems absent in the conventional power grid [3]. The integration of DGUs in the distribution network changes the levels and paths of fault current, leading to the malfunction of protective devices (PDs) due to downstream faults (protection blinding) and sympathetic tripping [4], [5].

To deal with these protection problems, limiting both the penetration level and rating power of DGUs has been proposed [6], [7]. This approach relieves the problem but works against achieving high penetration of DG. In the same direction, another proposal is to disconnect all DGUs under a fault condition [8], which limits the impact of DG on the protection system. However, disconnecting DGUs from the power grid could cause a large power imbalance and even the collapse of the power grid in a high-penetration scenario. Furthermore, in order to deal with changes in the levels and paths of fault currents, several new protection strategies have been proposed. These strategies are a great solution to tackling these protection problems but at the expense of great investments such as new sensors, intelligent protection devices, and communication systems [9]-[11]. Other studies strategically locate and size the DGUs to reduce changes in the protection system [12]. In contrast, an existing protection system may be configured optimally for a specific penetration level [13], [14]. Another approach is to limit the fault current contribution of DGUs by different types of fault current limiters (FCLs). Superconducting FCL (SFCL) and nonsuperconducting FCL (NSFCL) can be found in the literature as dedicated devices to limit the fault current [15].

Recent papers propose a control-based FCL to limit the fault current contribution of DGUs. References [16] and [17] propose to modify the control objective if the current injected by the DGU exceeds a certain threshold. It goes from controlling the voltage and frequency under normal operating conditions to regulating the current injected by the DGU

Manuscript received: May 2, 2021; revised: October 11, 2021; accepted: December 28, 2021. Date of CrossCheck: December 28, 2021. Date of online publication: May 26, 2022.

This work was supported in part by the Universidad Nacional de La Plata (UNLP) Project I255, in part by Consejo Nacional de Investigaciones Científicas y Técnicas (CONICET) PIPN° 112-2015-0100496CO, and in part by the Agencia Nacional de Promoción Científica y Tecnológica (ANPCyT) PICT N° 2015-2257.

P. E. Muñoz (corresponding author), R. J. Mantz, and S. A. González are with Instituto LEICI, UNLP, CONICET, La Plata 1900, La Plata, Argentina, and R. J. Mantz is also with the Commission of Scientific Researches of the Buenos Aires Province (CICpBA), La Plata, Argentina (e-mail: pablo_e. m@hotmail.com; mantz@ing.unlp.edu.ar; sag@ing.unlp.edu.ar).

DOI: 10.35833/MPCE.2021.000268

to a value of twice the nominal current under a faulty condition. Reference [18] proposes a virtual-impedance-based FCL to limit the fault current contribution of a DGU. Reproducing the behavior of a traditional FCL, a virtual impedance is connected in series with the DGU output when detecting a fault by comparing the output current with a threshold. Meanwhile, in normal operation, the virtual impedance is kept to be zero. The effect of this mechanism on the control loop is that the voltage loop reference is adjusted to be a suitable value so as not to exceed the current limit value.

Limiting the fault current contribution of DGUs can be stated as a constrained control problem [19]. In [16]-[18], controllers are designed without considering constraints, then modifications are introduced into the control loop to consider the constraints. In this paper, constraints are considered from the beginning of the design process as a closed-loop solution. To this end, the controller is stated as a constrained optimization problem, allowing considering the current limit explicitly in the design process. This current limit results in a nonlinear constraint, then a linear approximation is proposed. Thus, a model-based predictive controller (MPC) in the current control loop of a DGU is proposed and evaluated. The constraints on the currents are considered explicitly in the control loop that regulates them. Therefore, currents are quickly confined within the constraints. Moreover, with the predictive characteristics of the controller, it is not necessary to compare the DGU currents with any threshold or change the control objectives. This property makes the design process of the controller simple.

This paper is organized as follows. Section II presents the arising problem from DGUs on the protection system. Section III describes the conventional operation mode of DGU to evaluate the proposal. Section IV explains the proposed control-based FCL. Section V shows the simulation results for the different cases stated in Section II. Finally, in Section VI, the conclusions are presented.

II. Arising Problems From DGUs on Protection System

When a failure occurs in the power grid, the smaller possible portion of the network through the PDs must be isolated. The coordination between PDs is achieved by tunning the threshold current and action time. Action time is a function of the fault current threshold for inverse-time overcurrent relays, and the characteristics depend on specific PD type, according to the IEEE C37.112 standard, as shown in Appendix A.

After setting PDs, the connection of DGUs in the network can produce coordination loss and/or sensitivity loss between PDs. The miscoordination of PDs may cause false relay trips and disconnection of a greater network area, while the sensitivity loss may prevent or delay the isolation of the fault. As a consequence, delayed fault isolation will degrade the power quality. The impact of DG on the protection coordination and/or sensitivity depends on the network load, the location and operation modes of the DGUs, and fault location [20], [21].

Different effects caused by DG on the protection system are illustrated in Fig. 1, where V_s, Z_s, and I_s are the voltage, impedance, and current of the main grid, respectively; V_{dg}, Z_{dg}, and I_{dg} are the voltage, impedance, and current of the DGU, respectively; and Z_{load} is the impedance load. These effects are described below.

1) Protection blinding due to downstream faults: in the scenario shown in Fig. 1(a), consider that the PD is set previously to the connection of DGU. When a fault occurs at the load side, the current measured by PD is only part of the total fault current since $I_f = I_s + I_{dg}$, and only I_s passes through PD. Therefore, if I_{dg} is large enough, PD may act with inadmissible delay or even not act due to insufficient current when the feeder is at fault.

2) Sympathetic tripping: in the scenario shown in Fig. 1(b), assume that PD1 and PD2 are set previously to the connection of DGU. So, when a fault occurs in feeder2, the PD that must act is PD2. If the DGU is connected to feeder1, the direction of the current through PD1 may change, and if the DGU fault current is large enough, PD1 could be activated. If this happens, unreasonable electrical interruption may occur in the healthy feeder, reducing the system reliability.

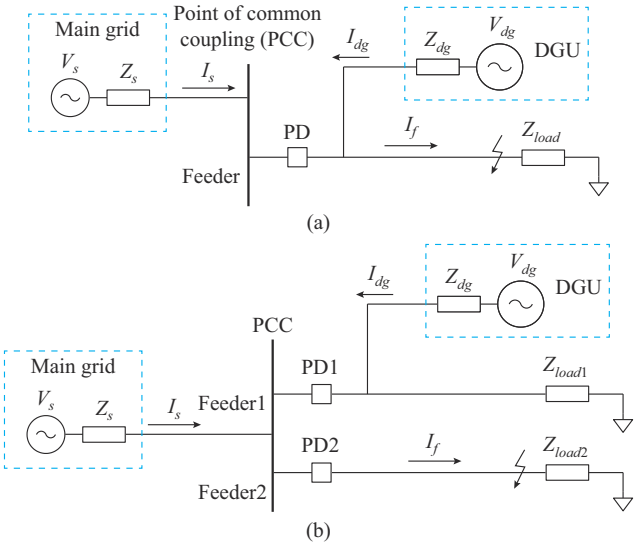

Fig. 1. Different effects caused by DG on protection system. (a) Malfunction of PD due to downstream fault. (b) Sympathetic tripping of PD1.

III. Conventional Operation Mode of DGU

Typically, DGUs are controlled to behave as a current source. Its fault current contribution depends on the fault location and the penetration level, size, type, and technology of the DGU. Generally, the inverters used in DGUs are designed to be able to support the power grid during transitory disturbances. In the worst case, if the fault current contribution continues for more than half a cycle [22], it typically does not exceed two times the steady-state current rating of the inverter [23].

In order to evaluate the proposal, a DGU connected to the network by a full-scale voltage source inverter (VSI) is considered, as shown in Fig. 2, where L_f, C_f, and R_f are the filter inductor, capacitor, and resistor, respectively; v and i are the voltage and current, respectively; θ is the voltage phase used to synchronize the reference frame; P and Q are the active and reactive power, respectively; ω^* and v_o^* are the nominal system frequency and the nominal voltage output, respec-

tively; ω and v_o are the system frequency and the voltage amplitude, respectively; P^* and Q^* are the active and reactive power references, respectively; m and n are the droop slopes; the subscripts c and o means for terminal converter and output quantities, respectively; and subscripts d and q represent d-axis and q-axis values, respectively. The VSI operates as a grid-supporting converter [2], which means that the DGU adjusts its active and reactive power to contribute to regulating both voltage amplitude and frequency. Figure 2 shows the overall control block diagram with two loops, i.e., an internal loop that regulates the current injected by the converter (current control loop) and an external loop that regulates the power that the converter exchanges with the power grid (droop control loop) generating the current references i_{cd}^* and i_{cq}^* for the inner loop. Note that, as stated above, our proposal relies on modifying the current control loop. So, it is applicable regardless of the operation mode of DGU since the current control loop is presented in all operating modes. In Fig. 2, PWM stands for pulse width modulation and PLL stands for phase-locked loop.

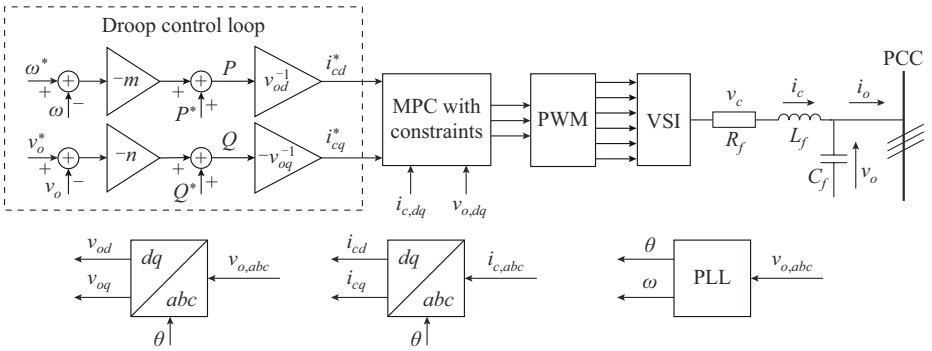

Fig. 2. Overall control block diagram with two loops.

The following droop laws are implemented in the droop control loop:

$$\begin{cases} P = -m(\omega - \omega^*) + P^* \\ Q = -n(v_o - v_o^*) + Q^* \end{cases} \tag{1}$$

Regarding the current control loop, it is typically implemented in d-q synchronous reference frame using proportional integral (PI) controllers. The reference frame is synchronized with the phase of the output voltage estimated by PLL. In this paper, to control and limit the DGU current contribution, the current control loop is considered as a multivariable system, where the converter current i_c is constrained to not exceed a predefined value, i.e., $i_c = \sqrt{i_{cd}^2 + i_{cq}^2} \le I_{\max}$, where i_{cd} and i_{cq} are the i_c components in the d-axis and q-axis, respectively.

IV. Proposed Control-based FCL

The MPC objective is to find the control action trajectory which optimizes the behavior of the system output, verifying the constraints imposed on the inputs, outputs, and/or states using a dynamic model to predict system behavior [24]. The control action is optimal in the sense that it minimizes a cost function subject to constraints. The optimization process is carried out within a time window or prediction horizon of N_p forward samples, using the available information of system state at the beginning of the time window. The control action can change only N_c samples in the future, which is known as the control horizon, and satisfy $N_c < N_p$. In summary, the MPC has the following components: ① a dynamic model to predict the system behavior N_p forward samples; ② a cost function and a set of constraints to establish the desired behavior of the system; and ③ an optimization process to find N_c samples forward a control action that minimizes the cost function and verifies the constraints.

A. Current Control Loop: Prediction

The control loop through the MPC regulates the currents i_{cd} and i_{cq} injected by the DGU to the connection point PCC. This connection is made through a coupling impedance, as shown in Fig. 2. The PEC will adjust its voltage v_c according to the current over L_f, i.e., i_c. It is necessary to have a dynamic model that relates the currents (controlled variable) with the voltages generated by the PEC (manipulated variable) to implement the MPC control. From transforming the system to a d-q synchronous reference frame preserving the amplitude, the following model, which represents the dynamics of the system, is obtained as:

$$\begin{bmatrix} \dot{i}_{cd} \\ \dot{i}_{cq} \end{bmatrix} = \begin{bmatrix} -\frac{R_f}{L_f} & \omega \\ -\omega & -\frac{R_f}{L_f} \end{bmatrix} \begin{bmatrix} i_{cd} \\ i_{cq} \end{bmatrix} + \frac{1}{L_f} \begin{bmatrix} v_{cd} \\ v_{cq} \end{bmatrix} - \frac{1}{L_f} \begin{bmatrix} v_{od} \\ v_{oq} \end{bmatrix} \tag{2}$$

where v_{cd} and v_{cq} are the DGU voltage components in the d-axis and q-axis, respectively; v_{od} and v_{oq} are the v_o components in the d-axis and q-axis, respectively; and ω is considered constant and equal to its nominal value for the prediction model. The last term at the right side in (2) represents the impact of the network voltage on the dynamics and can be considered as a measurable disturbance.

The first step in the problem statement following [24] is to discretize the prediction model. Then, the model is rewritten in increments of the variables and expanded to incorporate integral action taken as outputs of the controlled variables i_{cd} and i_{cq}. Therefore, (2) adopts the general form as:

$$\begin{cases} \boldsymbol{x}[k+1] = \boldsymbol{A}\boldsymbol{x}[k] + \boldsymbol{B}\Delta\boldsymbol{u}[k] + \boldsymbol{W}\Delta\boldsymbol{d}[k] \\ \boldsymbol{y}[k] = \boldsymbol{C}\boldsymbol{x}[k] \end{cases} \tag{3}$$

where $\boldsymbol{A}$, $\boldsymbol{B}$, $\boldsymbol{W}$, and $\boldsymbol{C}$ are the dynamic, input, disturbance,

and output matrices of the expanded model (3); k is the sampling time instant; $\boldsymbol{x}[k]=[\Delta i_{cd}[k],\Delta i_{cq}[k],i_{cd}[k],i_{cq}[k]]^{\mathrm{T}}$ is the vector state; $\Delta\boldsymbol{u}[k]=[\Delta v_{cd}[k],\Delta v_{cq}[k]]^{\mathrm{T}}$ is the manipulated variable; $\Delta\boldsymbol{d}[k]=[\Delta v_{od}[k],\Delta v_{oq}[k]]^{\mathrm{T}}$ is the measurable disturbance; and $\boldsymbol{y}=[i_{cd},i_{cq}]^{\mathrm{T}}$ is the output. The variable increments are defined as:

$$\begin{cases}\Delta i_{cd,q}[k]=i_{cd,q}[k]-i_{cd,q}[k-1]\\ \Delta v_{cd,q}[k]=v_{cd,q}[k]-v_{cd,q}[k-1]\\ \Delta v_{od,q}[k]=v_{od,q}[k]-v_{od,q}[k-1]\end{cases}\tag{4}$$

Based on the expanded model (3), the next step is to predict the evolution of states and outputs of N_p forward samples as a function of the manipulated variable $\Delta\boldsymbol{u}$. Since $\Delta\boldsymbol{u}$ varies over the control horizon, $\Delta\boldsymbol{u}[k_i]=0$ for $i=N_c+1,\ N_c+2,\ldots,\ N_p$. In this way, the output prediction $\boldsymbol{Y}$ is obtained as:

$$\boldsymbol{Y}=\boldsymbol{F}\boldsymbol{x}[k_i]+\boldsymbol{\Phi}\Delta\boldsymbol{U}+\boldsymbol{\Psi}\Delta\boldsymbol{D}\tag{5}$$

$$\begin{cases}\boldsymbol{F}=\begin{bmatrix}\boldsymbol{CA} & \boldsymbol{CA}^2 & \boldsymbol{CA}^3 & \cdots & \boldsymbol{CA}^{N_p}\end{bmatrix}^{\mathrm{T}}\\ \boldsymbol{\Phi}=\begin{bmatrix}\boldsymbol{CB} & \boldsymbol{0} & \cdots & \boldsymbol{0}\\ \boldsymbol{CAB} & \boldsymbol{CB} & \cdots & \boldsymbol{0}\\ \boldsymbol{CA}^2\boldsymbol{B} & \boldsymbol{CAB} & \cdots & \boldsymbol{0}\\ \vdots & \vdots & & \vdots\\ \boldsymbol{CA}^{N_p-1}\boldsymbol{B} & \boldsymbol{CA}^{N_p-2}\boldsymbol{B} & \cdots & \boldsymbol{CA}^{N_p-N_c}\boldsymbol{B}\end{bmatrix}\\ \boldsymbol{\Psi}=\begin{bmatrix}\boldsymbol{CW} & \boldsymbol{0} & \cdots & \boldsymbol{0}\\ \boldsymbol{CAW} & \boldsymbol{CW} & \cdots & \boldsymbol{0}\\ \boldsymbol{CA}^2\boldsymbol{W} & \boldsymbol{CAW} & \cdots & \boldsymbol{0}\\ \vdots & \vdots & & \vdots\\ \boldsymbol{CA}^{N_p-1}\boldsymbol{W} & \boldsymbol{CA}^{N_p-2}\boldsymbol{W} & \cdots & \boldsymbol{CW}\end{bmatrix}\\ \Delta\boldsymbol{U}=[\Delta\boldsymbol{u}[k_i] \quad \Delta\boldsymbol{u}[k_i+1] \quad \cdots \quad \Delta\boldsymbol{u}[k_i+N_c-1]]^{\mathrm{T}}\\ \Delta\boldsymbol{D}=[\Delta\boldsymbol{d}[k_i] \quad \Delta\boldsymbol{d}[k_i+1] \quad \cdots \quad \Delta\boldsymbol{d}[k_i+N_p-1]]^{\mathrm{T}}\end{cases}\tag{6}$$

where $\Delta\boldsymbol{U}$ is the optimal control sequence that minimizes $\boldsymbol{J}$ and satisfies the constraints.

B. Current Control Loop: Cost Function and Optimization

The goal of MPC is to achieve that the system output prediction is as close as possible to the reference signal r_s, satisfying all the constraints within the prediction horizon. To carry this out, the following optimization problem is stated as:

$$\begin{cases}\boldsymbol{J}=(\boldsymbol{R}_s-\boldsymbol{Y})^{\mathrm{T}}\boldsymbol{Q}(\boldsymbol{R}_s-\boldsymbol{Y})+\Delta\boldsymbol{U}^{\mathrm{T}}\bar{\boldsymbol{R}}\Delta\boldsymbol{U}\\ \text{s.t. } \boldsymbol{y}_k\in\mathcal{Y}\\ \quad\ \Delta\boldsymbol{u}_k\in\mathcal{U}\end{cases}\tag{7}$$

where $\boldsymbol{Q}$ is the matrix that must be positive semi-definite and weighs the outputs tracking error, and can be designed to give priorities, which is chosen as diagonal; $\bar{\boldsymbol{R}}$ is the matrix that must be positive definite, and is chosen as $\bar{\boldsymbol{R}}=r_w\boldsymbol{I}_{N_c\times N_c}$, where $r_w\geq 0$ and it is used as a design parameter for the desired closed-loop behavior, e.g., the settling time; $\mathcal{Y}$ and $\mathcal{U}$ are the output and input constraint sets, respectively; and $\boldsymbol{Y}$ is the output prediction. The reference signal is assumed to remain constant within the prediction horizon, hence $\boldsymbol{R}_s^{\mathrm{T}}=[1,1,\ldots,1]_{1\times N_p}\boldsymbol{r}_s[k_i]$. The first term in (7) reflects the objective of minimizing the error between the output prediction $\boldsymbol{Y}$ and the reference, and the second term in (7) penalizes the control action increment.

Finally, substituting (5) into (7) and considering $\mathcal{Y}$ and $\mathcal{U}$ polyhedral sets, i.e., linear constraints, the optimization problem (7) can be transformed into a quadratic program (QP) as:

$$\begin{cases}\min\limits_{\Delta\boldsymbol{U}}\ \{\boldsymbol{J}=\bar{\boldsymbol{J}}+\Delta\boldsymbol{U}^{\mathrm{T}}\boldsymbol{H}\Delta\boldsymbol{U}+2\Delta\boldsymbol{U}^{\mathrm{T}}\boldsymbol{\Phi}^{\mathrm{T}}\boldsymbol{Q}(\boldsymbol{F}\boldsymbol{x}[k_i]+\boldsymbol{\Psi}\Delta\boldsymbol{D}-\boldsymbol{R}_s)\}\\ \text{s.t. } \boldsymbol{M}\Delta\boldsymbol{U}\leq\boldsymbol{\gamma}\end{cases}\tag{8}$$

where $\bar{\boldsymbol{J}}$ is independent of $\Delta\boldsymbol{U}$, which does not affect the optimal solution and can be neglected; $\boldsymbol{H}$ is the Hessian matrix of the QP and $\boldsymbol{H}=\boldsymbol{\Phi}^{\mathrm{T}}\boldsymbol{Q}\boldsymbol{\Phi}+\bar{\boldsymbol{R}}$; and $\boldsymbol{M}$ and $\boldsymbol{\gamma}$ are a matrix and a vector of compatible dimensions, respectively. If the Hessian matrix is positive definite, the QP is convex. Note that $\boldsymbol{H}$ is positive definite since $\bar{\boldsymbol{R}}>\boldsymbol{0}$. In this paper, the QP is solved with Hildreth's procedure, which is iterative and does not require the inversion of matrices. Therefore, in case of conflict between constraints, Hildreth's procedure yields a compromise solution. The above is one of the advantages of this algorithm since it can automatically deal with an ill-conditioned problem [24].

C. Current Control Loop: Constraints

The objective is to limit the current of the converter so that it does not exceed a predefined value $I_{\max}$, i.e., $i_c\leq I_{\max}$. Since the d-q transformation preserves the amplitude, the previous inequality can be written as a function of the current components $i_c=\sqrt{i_{cd}^2+i_{cq}^2}\leq I_{\max}$, describing a circle of radius $I_{\max}$ in the i_{cd}-i_{cq} plane. This results in a nonlinear constraint, and the optimization problem cannot be written as (8). Then, it is proposed to approximate the circle by a polygon. The more sides the polygon has, the better it approximates the circumference. However, the number of linear constraints increases with the number of sides. Therefore, there is a trade-off between how conservative the approximation is and the number of resulting linear constraints. In this paper, an octagon is proposed to approximate the nonlinear constraint where 8% of $I_{\max}$ is lost in the worst case, as shown in Fig. 3. In this way, eight linear inequalities are obtained instead of one nonlinear inequality.

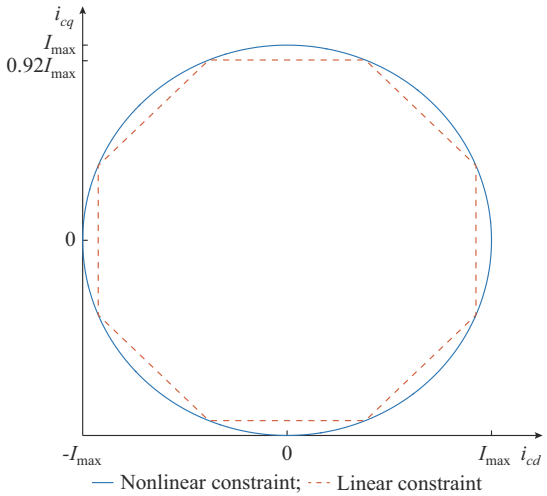

Fig. 3. Current constraint.

The proposed procedure is as follows. The constraints that define the octagon can be written in a general way as:

$$\xi_1 i_{cd} + \xi_2 i_{cq} \le \xi_3 I_{\max} \tag{9}$$

where ξ_1, ξ_2, and ξ_3 are the constant parameters depending on the ordinate at the origin and the slope of the lines forming the octagon. Then, the constraints are verified only in the first sample of $\Delta \boldsymbol{U}$, which is the only one applied to the system. In this way, the constraint statement is simplified, and the computational cost of the optimization is reduced. Therefore, (9) using the expanded model (3) without disturbance can be written as:

$$\begin{aligned}\xi_1[\boldsymbol{A}(1,:)x[k_i] + \boldsymbol{B}(1,:)\Delta \boldsymbol{U}[k_i]] + \\ \xi_2[\boldsymbol{A}(2,:)x[k_i] + \boldsymbol{B}(2,:)\Delta \boldsymbol{U}[k_i]] \le \xi_3 I_{\max}\end{aligned} \tag{10}$$

where the notation $(i,:)$ represents the i^{th} row of the matrix. Finally, by rewriting (10), the inequality constraint is obtained as (11) and is in the form of (8).

$$\underbrace{[\xi_1 \quad \xi_2]\boldsymbol{B}}_{M} \Delta \boldsymbol{U}[k_i] \le \underbrace{\xi_3 I_{\max} - [\xi_1 \quad \xi_2]\boldsymbol{A}\boldsymbol{x}[k_i]}_{\gamma} \tag{11}$$

Note that $I_{\max}$ can be chosen in accordance with the particularities of the system and even be changed according to the state of the system.

V. Simulation Results

Figure 4 shows the test network (medium voltage) considered to evaluate the proposed control-based FCL, in which the adverse effects of DG on the protection system are presented. Line impedance [2] is $(0.161 + j0.190)\,\Omega$/km. Coupling filter parameters of the DGU are $R_f = 0.038\,\Omega$, $L_f = 1.52$ mH, and $C_f = 20\,\mu$F. This test network exhibits the problems stated in Section II. It is considered as an original network (black line network) formed by two feeders connected to the PCC. Feeder1, with a length of 60 km, connects the load to the substation. Feeder2, with a length of 20 km, connects the load from PCC. Both feeders have an inverse time overcurrent relay (PD1 and PD2), which follows the law shown in Appendix A. One DGU is connected 10 km away from PCC (blue line network), which operates as explained in Section III with the proposed current control loop presented in Section IV. Table I shows the typical parameters for the configuration of the PDs.

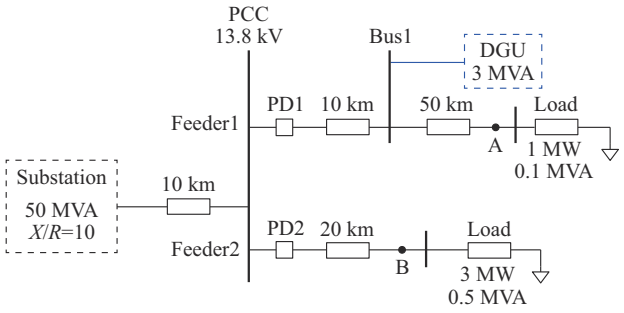

Fig. 4. Test network.

To evaluate the impact of DG on the protection system, two scenarios are considered. In the first scenario called protection blinding, a short circuit occurs at point A on feeder1. In the second scenario called sympathetic tripping, a fault at point B on feeder2 is studied. In each scenario, three simulation conditions are performed: ① without DGU; ② with DGU; and ③ with DGU and FCL.

TABLE I
PDs Configuration

PD	Curve characteristic	*TD*	I_{th} (A)
PD1	Extremely inverse	0.15	90
PD2	Extremely inverse	0.15	275

To tune the proposed control-based FCL, a sampling period of $T_m = 1 \times 10^{-4}$ is used to discretize the model (2) with $N_p = 10$, $N_c = 3$, $r_w = 1$, and $\boldsymbol{Q} = \text{diag}\{1, 10\}$. The choice of $\boldsymbol{Q}$ means that reactive power injection has the priority over active power injection, which is in accordance with the network codes.

Regarding the fault current limitation, it is a common practice to limit the current to twice its rated value during a fault [16], [17]. In order to highlight the flexibility and potential of the proposed control-based FCL, it is proposed to limit the fault current contribution of the DGU according to the severity of the abnormality [25].

$$I_{\max} = \begin{cases} \dfrac{P^*}{0.88\,V^*} & V_{bus1} \ge 0.88\,V^* \\ V_{bus1}\dfrac{P^*}{(0.88\,V^*)^2} & V_{bus1} < 0.88\,V^* \end{cases} \tag{12}$$

where V^* is the nominal voltage; and V_{bus1} is the voltage at the connection point of the DGU, as shown in Fig. 4. In this way, if the DGU is located close to the fault location which produces the greatest impact on the protection system, the voltage sag experienced by the DGU is deeper. Therefore, its contribution to the fault current during the fault is reduced without limiting its power contribution under normal conditions.

A. Scenario 1: Protection Blinding

In this scenario, a balanced short circuit is considered at point A, as shown in Fig. 4, which occurs at $t = 1$ s. The transient responses of the currents injected by the DGU, with and without FCL, are shown in Fig. 5(a) and (b), respectively. Without FCL, the DGU increases its current contribution without exceeding the limit of twice its nominal current, i.e., 355 A in this scenario, so the typical FCL that limits the current to twice the rated current would not act in this case. When the proposed control-based FCL is activated on the DGU, the current is quickly confined within the constraint despite the suddenness of the disturbance, which causes a practically instantaneous voltage drop. Figure 6(a) shows the current transient in the i_d-i_q plane, and Fig. 6(b) shows the time evolution of its components. Points A to D pointed out in Fig. 6(a) agrees to the time instants A to D pointed out in Fig. 6(b). Note that the constraint under normal conditions is exceeded only at the initial instant for less than half cycle (< 1 ms). So, the current is limited within the constraints during voltage sag in less than a network cycle (< 15 ms). This

fast response avoids that any protection, either the PDs of the system or DGU protection, acts due to transient peaks. Regarding this, the benefit of the proposed control-based FCL is twofold: not only avoids the protection blinding but also guarantees that the DGU never goes out of service due to overcurrent.

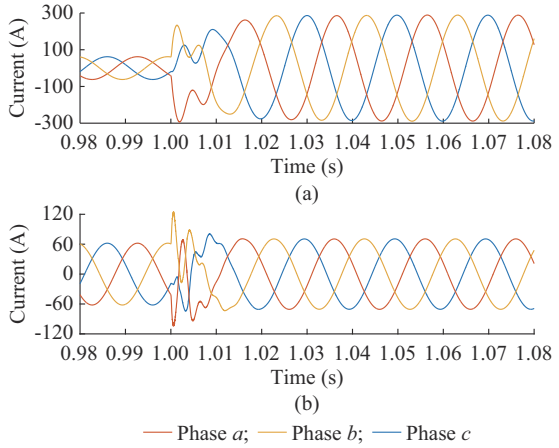

Fig. 5. DGU current. (a) Without FCL. (b) With FCL.

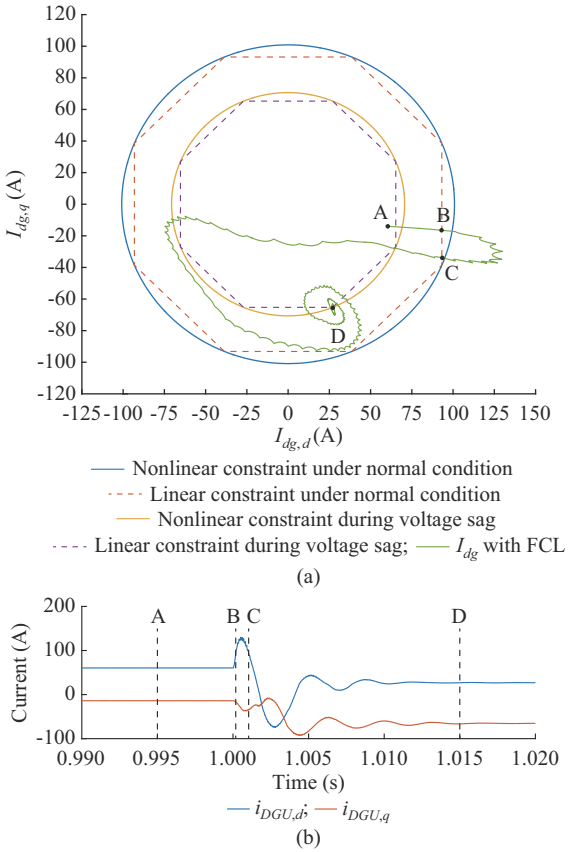

Fig. 6. DGU current component. (a) i_d-i_q plane. (b) $i_{DGU,d}$ and $i_{DGU,q}$.

Figure 7 shows the root mean square (RMS) current through PD1. It can be observed that the current through PD1 quickly increases to seven times the nominal current when the fault occurs, and PD1 acts in 0.3 s approximately. The solid red line shows the case where the DGU is connected to the power grid without FCL. Note that, when the fault occurs, the current through PD1 increases to five times the rated current. These approximately 100 A less are due to fault current contribution from the DGU, thus delaying PD1 to act, practically doubling the acting time of PD1 without DGU, i.e., 0.6 s. The solid yellow line corresponds to the case where the DGU is connected to the power grid and has the proposed control-based FCL. The fault current through PD1 in this case is closer to the case where there is no DGU (solid blue line), and it delays only about three more network cycles (0.06 s) to operate, reducing the protection blinding.

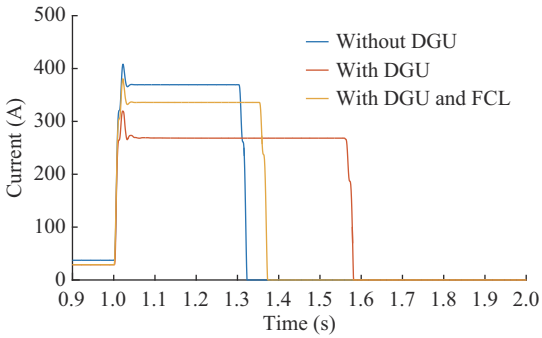

Fig. 7. RMS current through PD1.

Figure 8 shows the voltage and frequency at the PCC under the same three simulation conditions. From Fig. 8(a), it can be observed that the voltage drops by twice the time when the fault current of the DGU is not limited. Therefore, this extended voltage dip could lead to both malfunction or damage of sensitive load in feeder2. Comparing the frequency responses for the different cases, it can be observed from Fig. 8(b) that the frequency transient is practically the same when the fault current of the DGU is limited.

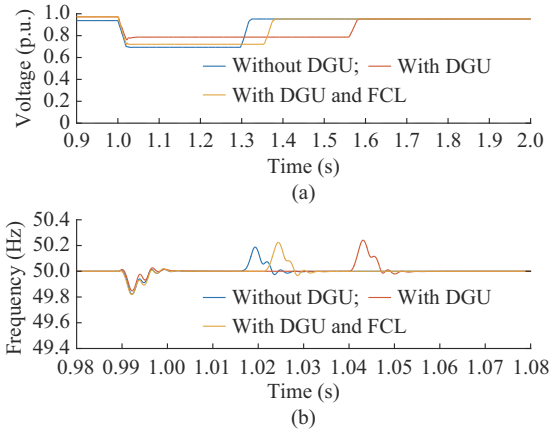

Fig. 8. Voltage and frequency at PCC. (a) Voltage. (b) Frequency.

Therefore, the impact of the DGU on the protection system is significantly reduced when the fault current limitation in the DGU is considered, which is important in order to maintain power quality in healthy feeders.

B. Scenario 2: Sympathetic Tripping

In this scenario, a balanced short circuit occurs at point B in feeder2, as shown in Fig. 4. The transient responses of

the currents injected by the DGU, with and without FCL, are shown in Fig. 9. Again, without FCL, the DGU increases its current contribution without exceeding the limit of twice its nominal current, so the typical FCL that limits the current to twice the nominal current would not act in this scenario. When the proposed control-based FCL on DGU is activated, the current is quickly confined within the constraint. Note that in this scenario, the constraint during the voltage sag is even less than that under normal conditions since the voltage sag is deeper than that in scenario 1.

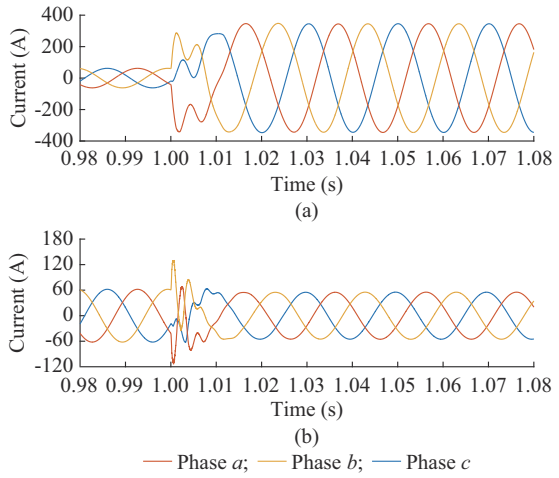

Fig. 9. Transient responses of currents injected by DGU. (a) Without FCL. (b) With FCL.

Figure 10 shows the current through PD1 and PD2 for the three simulation cases. It can be observed that if the fault current injected by the DGU is not limited (solid red line), PD1 is activated before PD2 isolates the fault (approximately at $t=$ 1.65 s). Then, the service in the healthy feeder is interrupted. Therefore, in this scenario, limiting the DGU fault current is essential to avoid sympathetic tripping.

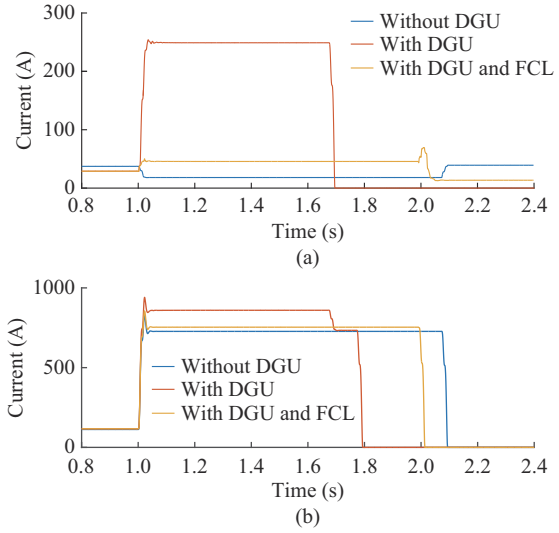

Fig. 10. Current through PD1 and PD2 for three simulation cases. (a) PD1. (b) PD2.

Figure 11 shows the voltage and frequency at bus 1 in feeder1. It can be noted that when no limit exists in the fault current of DGU, after the activation of PD1, both the frequency and the voltage drop to zero. This is due to that feeder1 without power source is able to impose the voltage and frequency. In this case, the DGU must go out of service. PD1 is not activated when limiting the DGU fault current. Thus, once the fault is isolated by the action of PD2 (approximately at $t=2$ s), both the voltage and frequency return to their normal values. This is similar to the case in which the DGU is not connected.

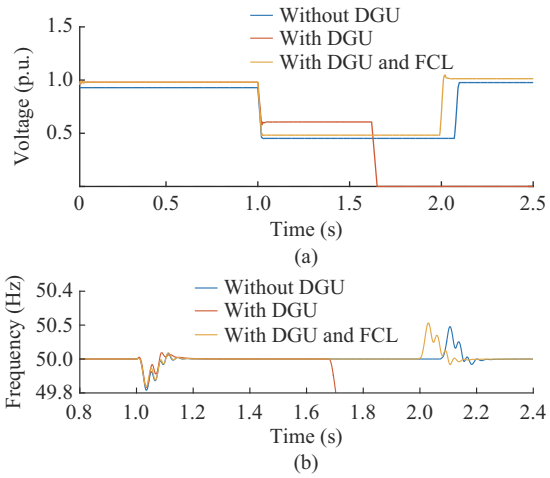

Fig. 11. Voltage and frequency at bus 1 in feeder1. (a) Voltage. (b) Frequency.

VI. Conclusion

In this paper, a control-based FCL is proposed to minimize the impact of DG on the protection system. The FCL is based on predictive control without altering the topology of the control loop, implementing some kind of fault detector, or changing the control objectives. Therefore, it is easier to understand and tune in compared with other strategies found in the literature. Moreover, this is a closed-loop solution that considers the constraints as a control objective directly in the current control loop. Thus, it is possible to impose the current constraints quickly, in less than 1 ms, which is a substantial improvement compared with other proposals. This fast response of the proposed strategy is crucial to avoid that any protection, either the PDs of the system or protections of the DGU, acts due to transient peaks. Therefore, the proposed control-based FCL not only reduces the impact of the DGU on the protection system but also allows the DGU to ride through the fault connected to the power grid. Both protection blinding and sympathetic tripping scenarios are studied and simulated. The simulation results show that the proposed strategy can substantially diminish the deterioration in the protection system.

Appendix A

Overcurrent relays used as PDs are classified according to its characteristics: ① instantaneous; ② definite-time; and ③ inverse-time. The first two act when the current exceeds a predefined threshold instantaneously in the first case and after a predefined time in the second case. The inverse-time overcurrent relays operate in a time defined as [26]:

$$t(I)=TD\cdot\left(\frac{A}{M^{P}-1}+B\right) \tag{A1}$$

where t is the time in which the device acts; and $M=I/I_{th}$ is the multiples of the threshold current I_{th}; and TD is the time dial setting. Constants A, B, and P are adjusted to obtain a specific desired curve. The IEEE C37.112 standard establishes three classes: moderately inverse, very inverse, and extremely inverse. The values of standard constants are shown in Table AI.

TABLE AI
VALUES OF STANDARD CONSTANTS

Curve characteristic	A	B	P
Moderately inverse	0.0515	0.1140	0.02
Very inverse	19.6100	0.4910	2.00
Extremely inverse	28.2000	0.1217	2.00

REFERENCES

[1] T. Ackermann, G. Andersson, and L. Söder, "Distributed generation: a definition," *Electric Power Systems Research*, vol. 57, no. 3, pp. 19-204, Apr. 2001.

[2] J. Rocabert, A. Luna, F. Blaabjerg *et al*., "Control of power converters in AC microgrids," *IEEE Transactions on Power Electronics*, vol. 27, no. 11, pp. 4734-4749, Nov. 2012.

[3] S.-E. Razavi, E. Rahimi, M. S. Javadi *et al*., "Impact of distributed generation on protection and voltage regulation of distribution systems: a review," *Renewable and Sustainable Energy Reviews*, vol. 105, pp. 157-167, May 2019.

[4] P. T. Manditereza and R. Bansal, "Renewable distributed generation: the hidden challenges–a review from the protection perspective," *Renewable and Sustainable Energy Reviews*, vol. 58, pp. 1457-1465, May 2016.

[5] S. Beheshtaein, M. Savaghebi, J. C. Vasquez *et al*., "Protection of AC and DC microgrids: challenges, solutions and future trends," in *Proceedings of IECON 2015-41st Annual Conference of the IEEE Industrial Electronics Society*, Yokohama, Japan, Nov. 2015, pp. 5253-5260.

[6] J. Chen, R. Fan, X. Duan *et al*., "Penetration level optimization for DG considering reliable action of relay protection device constrains," in *Proceedings of 2009 International Conference on Sustainable Power Generation and Supply*, Nanjing, China, Apr. 2009, pp. 1-5.

[7] S. Chaitusaney and A. Yokoyama, "An appropriate distributed generation sizing considering recloser-fuse coordination," in *Proceedings of 2005 IEEE/PES Transmission & Distribution Conference & Exposition: Asia and Pacific*, Dalian, China, Aug. 2005, pp. 1-6.

[8] S. Conti, "Analysis of distribution network protection issues in presence of dispersed generation," *Electric Power Systems Research*, vol. 79, no. 1, pp. 49-56, Jan. 2009.

[9] L. Che, M. E. Khodayar, and M. Shahidehpour, "Adaptive protection system for microgrids: protection practices of a functional microgrid system," *IEEE Electrification Magazine*, vol. 2, no. 1, pp. 66-80, Mar. 2014.

[10] V. A. Papaspiliotopoulos, G. N. Korres, V. A. Kleftakis *et al*., "Hardware-in-the-loop design and optimal setting of adaptive protection schemes for distribution systems with distributed generation," *IEEE Transactions on Power Delivery*, vol. 32, no. 1, pp. 393-400, Dec. 2017.

[11] A. M. Tsimtsios and V. C. Nikolaidis, "Towards plug-and-play protection for meshed distribution systems with DG," *IEEE Transactions on Smart Grid*, vol. 11, no. 3, pp. 1980-1995, Oct. 2019.

[12] H. Zhan, C. Wang, Y. Wang *et al*., "Relay protection coordination integrated optimal placement and sizing of distributed generation sources in distribution networks," *IEEE Transactions on Smart grid*, vol. 7, no. 1, pp. 55-65, Apr. 2015.

[13] S. Javadian and M. Massaeli, "Fuzzy risk based method for optimal placement of protection devices in distribution networks with DG," in *Proceedings of 2016 IEEE Innovative Smart Grid Technologies-Asia (ISGT-Asia)*, Melbourne, Australia, Nov. 2016, pp. 838-843.

[14] S. M. Saad, N. E. Naily, J. Wafi *et al*., "An optimized proactive overcurrent protection scheme for modern distribution grids integrated with distributed generation units," in *Proceedings of 2018 9th International Renewable Energy Congress (IREC)*, Hammamet, Tunesia, Mar. 2018, pp. 1-6.

[15] M. Alam, M. Abido, and I. El-Amin, "Fault current limiters in power systems: a comprehensive review," *Energies*, vol. 11, no. 5, p. 1025, Apr. 2018.

[16] S. Beheshtaein, M. Savaghebi, J. M. Guerrero *et al*., "A secondary-control based fault current limiter for four-wire three phase inverter-interfaced dgs," in *Proceedings of IECON 2017-43rd Annual Conference of the IEEE Industrial Electroninc Society*, Beijing, China, Oct. 2017, pp. 2363-2368.

[17] S. Beheshtaein, M. Savaghebi, R. M. Cuzner *et al*., "Modified secondary-control-based fault current limiter for inverters," *IEEE Transactions on Industrial Electronics*, vol. 66, no. 6, pp. 4798-4804, Jul. 2019.

[18] X. Lu, J. Wang, J. M. Guerrero *et al*., "Virtual-impedance-based fault current limiters for inverter dominated AC microgrids," *IEEE Transactions on Smart Grid*, vol. 9, no. 3, pp. 1599-1612, May 2018.

[19] G. Goodwin, M. M. Seron, and J. A. De Doná, *Constrained Control and Estimation: an Optimisation Approach*. New York: Springer Science & Business Media, 2006.

[20] K. Jennett, F. Coffele, and C. Booth, "Comprehensive and quantitative analysis of protection problems associated with increasing penetration of inverter-interfaced DG," in *Proceedings of 11th IET International Conference on Developments in Power Systems Protection (DPSP 2012)*, Birmingham, UK, Apr. 2012, pp. 1-6.

[21] T. N. Boutsika and S. A. Papathanassiou, "Short-circuit calculations in networks with distributed generation," *Electric Power Systems Research*, vol. 78, no. 7, pp. 1181-1191, Jul. 2008.

[22] J. Keller and B. Kroposki, "Understanding fault characteristics of inverter-based distributed energy resources," National Renewable Energy Lab, Golden, CO, Tech. Rep. Jan. 2010.

[23] T. M. Masaud and R. D. Mistry, "Fault current contribution of renewable distributed generation: an overview and key issues," in *Proceedings of 2016 IEEE Conference on Technology for Sustainability*, Phoenix, USA, Oct. 2016, pp. 229-234.

[24] L. Wang, *Model Predictive Control System Design and Implementation Using MATLAB*. New York: Springer Science & Business Media, 2009.

[25] H. Yazdanpanahi, Y. Li, and W. Xu, "A new control strategy to mitigate the impact of inverter-based dgs on protection system," *IEEE Transactions on Smart Grid*, vol. 3, no. 3, pp. 1427-1436, Jul. 2012.

[26] G. Benmouyal, M. Meisinger, J. Burnworth *et al*., "IEEE standard inverse-time characteristic equations for overcurrent relays," *IEEE Transactions on Power Delivery*, vol. 14, no. 3, pp. 868-872, Jul. 1999.

Pablo E. Muñoz received the Engineer degree in automation and control from the Universidad Nacional de Quilmes (UNQ), Quilmes, Argentina, in 2017. He is currently working toward the Ph.D. degree from the Facultad de Ingeniería, Universidad Nacional de La Plata, at the Instituto LEICI (UNLP-CONICET), La Plata, Argentina, being supported by a research scholarship from the Consejo Nacional de Investigaciones Científicas y Técnicas (CONICET), Buenos Aires, Argentina. He is also working as a Teaching Assistant at control systems courses at UNQ. His current research interests include modeling and control for distributed generation and microgrid applications.

Ricardo J. Mantz is a Professor of automatic control at the Faculty of Engineering of the National University of La Plata (UNLP), La Plata, Argentina. He has been Official Member of the Commission of Scientific Researches of the Buenos Aires Province (CICpBA), La Plata, Argentina. He is with the Instituto LEICI (UNLP-CONICET), La Plata, Argentina. His main research interests include switched control systems, sliding mode control, and control of renewable energy conversion systems.

Sergio A. González received the Engineer degree in electronics, the M.Sc., and Ph.D. degrees from National University of La Plata (UNLP), La Plata, Argentina, in 1992, 2000, and 2010, respectively. Since 1993, he has worked on research activities at the Institute of Power Electronics, Instrumentation and Signal Processing of LEICI (UNLP-CONICET), La Plata, Argentina. Currently, he is a Professor of Power Electronics at the Faculty of Engineering of the UNLP and Science and Technical Department of the National University of Quilmes (UNQ), Quilmes, Argentina. His research interests include power electronics conversions in high and low power applications and applications of sustainable energy systems.